THE JOURNAL OF PHYSICAL CHEMISTRY B
A JOURNAL OF THE AMERICAN CHEMICAL SOCIETY

pubs.acs.org/JPCB

Article

Flow through Deformed Carbon Nanotubes Predicted by Rigid and Flexible Water Models

Bruno H. S. Mendonça,* Elizane E. de Moraes, Alexsandro Kirch, Ronaldo J. C. Batista, Alan B. de Oliveira, Marcia C. Barbosa, and Hélio Chacham

Cite This: *J. Phys. Chem. B* 2023, 127, 8634–8643

Read Online

ACCESS | Metrics & More | Article Recommendations

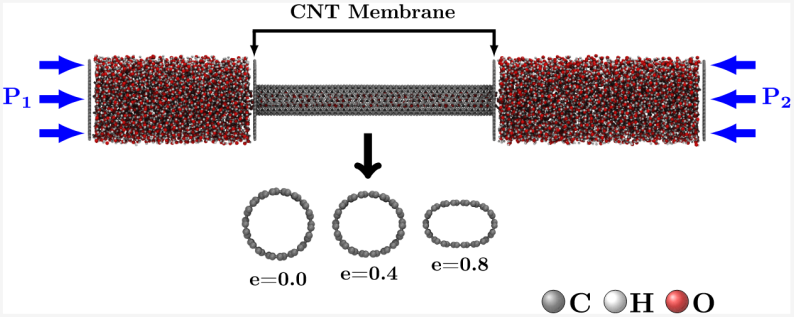

ABSTRACT: In this study, using nonequilibrium molecular dynamics simulation, the flow of water in deformed carbon nanotubes is studied for two water models TIP4P/2005 and simple point charge/FH (SPC/FH). The results demonstrated a nonuniform dependence of the flow on the tube deformation and the flexibility imposed on the water molecules, leading to an unexpected increase in the flow in some cases. The effects of the tube diameter and pressure gradient are investigated to explain the abnormal flow behavior with different degrees of structural deformation.

INTRODUCTION

Under spatial confinement, water exhibits unusual properties, and its flow velocity may be a thousand times faster than that predicted by hydrodynamics.[1−5] This characteristic is desirable for applications such as drug delivery[6,7] and biomimetic selective ionic transport.[8] Also, the ionic selectivity for water desalination[9,10] and energy storage,[11] where the enhanced flow rates would improve the device efficiency, accuracy, and throughput.

The large surface area-to-volume ratio inherent to the nanoscale plays a central role in the water transport properties.[2,12] From the experimental perspective, Qin et al.[3] observed that water velocity in carbon nanotubes (CNTs) decreases with increasing tube diameter; therefore, the obtained values ranged between 46 (1.6 nm) and 928 μ m/s (0.8 nm). Also, Secchi et al.[13] evaluated the fluid flow rate in nanochannels and observed that the slip length increases monotonically with the decrease in tube diameter. Compared to boron nitride tubes with similar diameters, the slip length observed in CNTs was approximately 100 times higher.

From the molecular modeling perspective, the water transport in nanotubes[14] was investigated with ab initio and classical molecular dynamics (MD). While the ab initio approach is limited by the number of atoms in the system, the classical results depend on reliable molecular models. In the case of water, various molecular models are available to reproduce the competing effects of hydrogen bonding and van der Waals interactions, which are responsible for water's anomalous properties.[15−37] The literature on more complex models for water, including polarization is vast and a number of bulk properties have been explored using them.[29−72] Here, we are looking for a more simplified picture that would help us understand the minimum mechanism behind the high mobility of confined water, which we believe can be represented by a combination of water−water and water−wall interaction, which preserves the dielectric constant and single file mobility. The rigid TIP4P/2005[17] and the flexible simple point charge/FH (SPC/FH)[16] are the most popular models with reliable results describing bulk properties.

The high mobility of confined water is relevant for improving desalination processes. For that purpose, it would be interesting to work with water models that provide good results both for the water mobility and dielectric constant.

Received: May 2, 2023
Revised: September 10, 2023
Published: September 27, 2023

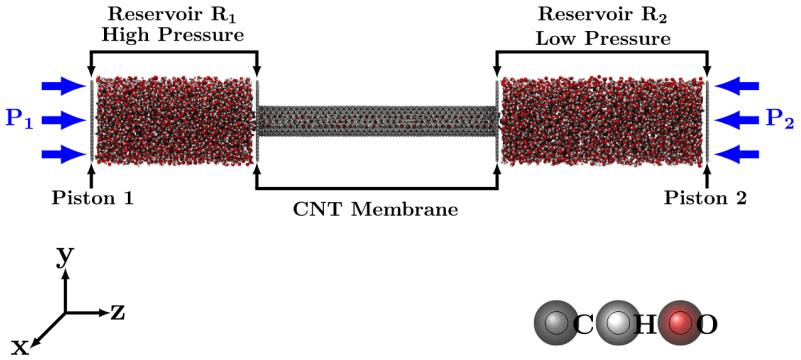

Figure 1. Snapshot of the model system composed of two reservoirs, R_1 and R_2, with water at different pressures and limited by graphene membranes of side lengths $L_x = L_y = 3$ nm connected to a CNT with length $L_z = 10$ nm and diameter d.

Even though the four points flexible TIP4P/2005f can be viewed as an improvement on the atomistic TIP4P/2005,[73] for these two quantities, the results are not particularly good.[74] The SPC flexible models, on the other hand, give good results when compared with the experiments.[75]

The SPC/FH model has been shown to accurately reproduce several properties of liquid water and has been widely used in the study of confined water in nanoscale environments, particularly with salt,[24,76] but little is known about its performance in describing fluid flow in a confined scenario. However, their transferability to the confined environment is currently under discussion, and comparative studies involving different molecular models may guide performance evaluation.

Most computer-based studies on fluid transport analyzed perfect cylindrical CNTs, and few works considered a more realistic description by including structural deformations.[77,78] As typical, the synthesis process may result in defective CNTs with vacancies and structural distortions[79,80] resulting from adsorbed functional groups or mechanical compression. Structural deformations may influence the flow velocity, shear stress, and effective viscosity.[81−83] Further studies on this topic may contribute to a more comprehensive understanding of mass transport in synthesized CNTs.

Recently, we compared the diffusion coefficient of atomistic, TIP4P/2005, water and flexible, SPC/H, water models when confined in carbon nanotubes.[84] Even though in the bulk, both models show a similar diffusion coefficient, we found that the diffusion coefficient under confinement is higher for the TIP4P/2005 water when compared with that of the SPC/FH water. This larger diffusion correlates with a greater number of hydrogen bonds.

We performed a systematic study to investigate the effect of structurally deformed CNTs on water transport properties within the classical nonequilibrium molecular dynamics simulations approach. The water flow rate was related to the tube chirality, diameter, and deformation level. We compared the results from rigid and flexible water models to evaluate their transferability to a confined environment context.

The remainder of this article is organized as follows. In the Model and Method section, we present the methodology used in this analysis and define the simulated models. In the Results and Discussion section, the discussion of the results is exposed. In the Conclusions section, we present the conclusions.

MODEL AND METHOD

Our system setup is similar to the molecular model proposed by Huang et al.,[85] where a nanotube connects two fluid reservoirs and enables the investigation of the fluid transport. The system is shown in Figure 1, and it is described as follows. Two reservoirs with water, R_1 and R_2, at different pressures, limited by two graphene membranes with size $L_x = L_y = 3$ nm are connected to a CNT with size length $L_z = 10$ nm and diameter d. The pressure at the two reservoirs is determined by two pistons, P_1 and P_2.

Outer graphene sheets on each reservoir play the role of pistons 1 and 2. The pressure on each piston is given by

$$P = \frac{F \cdot n}{A} \tag{1}$$

where F is the external force in the z direction applied to each atom in the graphene sheet, n is the number of carbon atoms, and A is the surface area. While the pressure in piston 1 ranges from 200 to 800 bar, piston 2 has a fixed value of 1 bar to impose a pressure gradient on the system.

Here, we study the armchair and zigzag nanotubes with diameters shown in Table 1, with armchair and zigzag displaying similar diameters for comparison. Our study considers two types of CNTs, i.e., perfect P(n,m) and kneaded K(n,m), as illustrated in Figure 2. The kneaded nanotubes K(n,m) are produced by uniformly deforming a perfect nanotube P(n,m) in the radial direction until the nanotube reaches an elliptical cylindrical shape with eccentricities equal to 0.4 and 0.8.[84,86−88]

Table 1. Parameters for the Simulated Perfect Carbon Nanotubes (e = 0.0) Armchairs and Zigzags

CNT	d (nm)
(7,7)	0.95
(12,0)	0.94
(9,9)	1.22
(16,0)	1.25
(12,12)	1.63
(21,0)	1.64

The water molecules are represented by two different models: the flexible SPC/FH[24] and the rigid TIP4P/2005.[17] The parameters considered for the water models were defined and are shown in Table 2. In this water model, the Lennard-Jones site is located on the oxygen atom, with parameters σ and ε. The charges of oxygen and hydrogen are q_O and q_H,

https://doi.org/10.1021/acs.jpcb.3c02889
J. Phys. Chem. B 2023, 127, 8634−8643

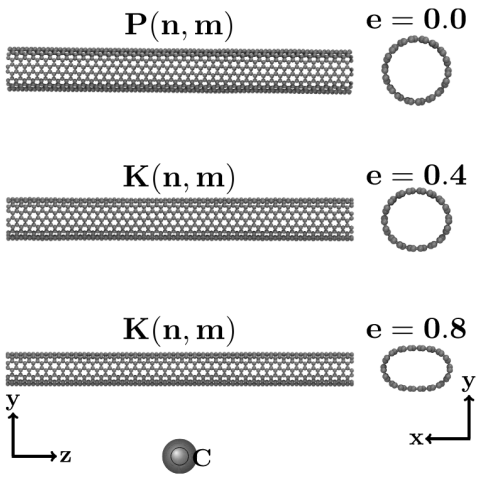

Figure 2. Snapshot of the perfect P(n,m) simulated carbon nanotubes with eccentricity equal to 0.0, and kneaded K(n,m) with eccentricities equal to 0.4 and 0.8.

Table 2. Force Field Parameters Used for Each of the Water Models

	TIP4P/2005	SPC/FH
ε_{OO} (kcal mol^{-1})	0.1852	0.1553
ε_{HH} (kcal mol^{-1})	0.0	0.0396
σ_{OO} (Å)	3.1589	3.188
σ_{HH} (Å)	0.0	0.65
q_O (e)	0.0	−0.8476
q_H (e)	0.5564	0.4138
q_M (e)	−1.1128	
d_{OM} (Å)	0.1546	
r_{OH} (Å)	0.9572	1.0
θ_{HOH} (deg)	104.52	109.4
k_{OH} (kcal mol^{-1} Å^{-2})		1108.580
k_θ (kcal mol^{-1} rad^{-2})		91.53

respectively. The TIP4P/2005 model places a negative charge q_M at a point M at a distance d_{OM} from the oxygen along the H−O−H bisector. The distance between the oxygen and the hydrogen sites is r_{OH}. The angle formed between hydrogen, oxygen, and another hydrogen atom is given by θ_{HOH}. For the flexible model SPC/FH, k_{OH} and k_θ are the potential depth parameters, and OH and θ are the reference bond length and angle, respectively.

The SHAKE[89] algorithm is employed to stabilize the molecule bonds and angles. The nanotube and the graphene sheets are modeled by the Lennard-Jones potential (LJ) considering fixed bond lengths and angles[90] with effective carbon−carbon interaction energy ε_{CC} = 0.086 kcal·mol^{-1} and an effective diameter of σ_{CC} = 3.4 Å.[4] The carbon−oxygen energy ε_{CO} = 0.11831 kcal·mol^{-1} and the effective carbon−oxygen diameter σ_{CO} = 3.28218 Å.[4] The Lorentz−Berteloth mixing rules provided the LJ crossing parameters.

We adopted the Large-scale Atomic/Molecular Massively Parallel Simulator (LAMMPS)[14] package to perform the simulations, with the Particle−Particle Particle-Mesh (PPPM) method to calculate long-range Coulomb interactions.[91]

The system's dynamics features were evaluated by considering the flow rate calculations as given by the equation

$$\phi_{H_2O} = A\nu \quad (2)$$

where A is the graphene layer area (34 × 34 Å^2) and ν is the water flow velocity acquired from the least-squares linear regression line fitted to the data cloud, which relates the average molecular displacement along the tube axis as a function of the time as taken from the MD trajectory file.

The simulation protocol involves the following steps:

1. Pre-equilibrium in the NVE ensemble with a 0.5 ns MD run to minimize system energy keeping the pistons frozen (net force equal to zero).
2. Forces are applied in the pistons in order to impose 1 bar in each system to reach the water equilibrium densities at 300 K. Equilibration in the NPT ensemble during 1.0 ns.
3. Pistons are freezed in the new equilibrium position. Equilibration in the NVT ensemble at 300 K controlled via the Nosé−Hoover thermostat[92] during 2.0 ns.
4. Nanopores are opened. Different forces are applied in each piston to mimic the pressure gradient. NPT ensemble during 10 ns at 300 K and different feed pressures.

RESULTS AND DISCUSSION

Water transport in carbon nanotubes is highly dependent on the diameter of the tubes.[84,86−88,93−96] Considering the high resistance to flow in the inlet and outlet regions of small-diameter CNTs, the flow rate and water molecule flux through the CNTs will decrease markedly with decreasing CNT diameters.[97] For small-diameter tubes, the size of the fluid particles becomes crucial and occupies a considerable portion of the determining mobility. However, for those with a larger diameter, these effects will diminish.[98,99] Some experimental data significantly suggest that the configuration of water in nanotubes can vary according to their diameters.[86−88,96,100,101]

Recently, Losey et al.,[102] studied the flow of water in CNTs for a variety of water models. They observed that the flux of water through CNTs depends on the diameter of the carbon nanotube. Although the magnitude of the flow rate depended on the water model, they were similar qualitatively. In this work, the same behavior is observed for perfect nanotubes P(n,m) with e = 0, for $P \leq 600$ bar as illustrated in Figures 3, 4, and 6.

Even though the flow decreases with the decrease of the diameter, the ratio between the flow obtained in the simulation and the value classical hydrodynamic predicts for diameters below 1 nm increases with the decrease of the diameter because in this regime the water flows in a stressless single line. This enhancement flow with the decrease of the diameter is larger for armchair than for the zigzag nanotubes.[103] This indicates that the spiral-like path of the water at armchair nanotubes exhibits less stress than the ring-like move of water at the zigzag nanotube. We test how this is affected by the deformation and the nature of the water model.

Figure 3a shows the flow rate as a function of pressure for the armchair (7,7) nanotube for the TIP4P/2005 model for the perfect and two cases of kneaded nanotubes. For perfect zigzag nanotubes and large pressure gradients, the increase of pressure increases the flow.[104] In the presence of any disturbance such as additional ions or asymmetric pressure, the behavior of the flow rate with pressure is monotonic.[105,106] This suggests that at small pressure gradients or in the presence of deformations, the flow rate is the result of a

https://doi.org/10.1021/acs.jpcb.3c02889
J. Phys. Chem. B 2023, 127, 8634−8643

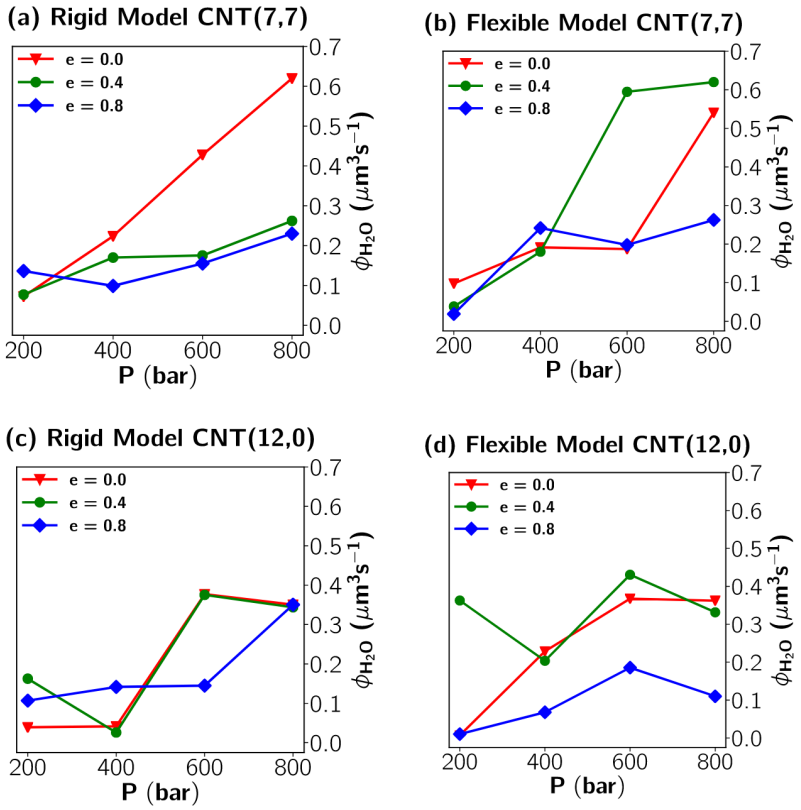

Figure 3. Flow rate as a function of the pressure gradient applied to the carbon nanotubes, (7,7) and (12,0), perfect P(n,m) with e = 0.0 and kneaded K(n,m) with e = 0.4 and 0.8 for rigid TIP4P/2005 and flexible SPC/FH water models.

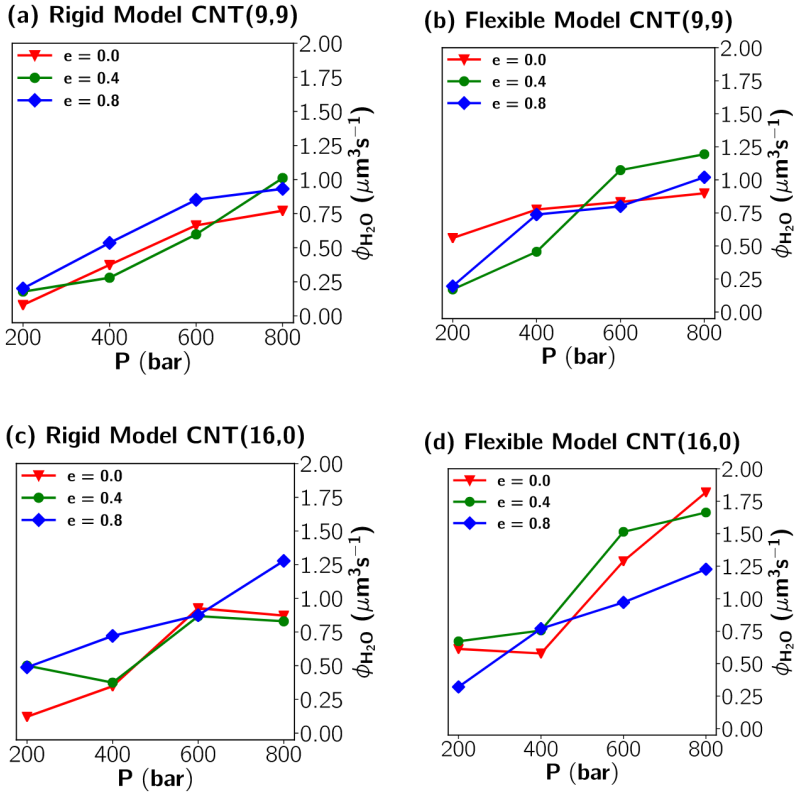

Figure 4. Flow rate as a function of the pressure gradient applied to the carbon nanotubes, (9,9) and (16,0), perfect P(n,m) with e = 0.0 and kneaded K(n,m) with e = 0.4 and 0.8 for rigid TIP4P/2005 and flexible SPC/FH water models.

https://doi.org/10.1021/acs.jpcb.3c02889
J. Phys. Chem. B 2023, 127, 8634−8643

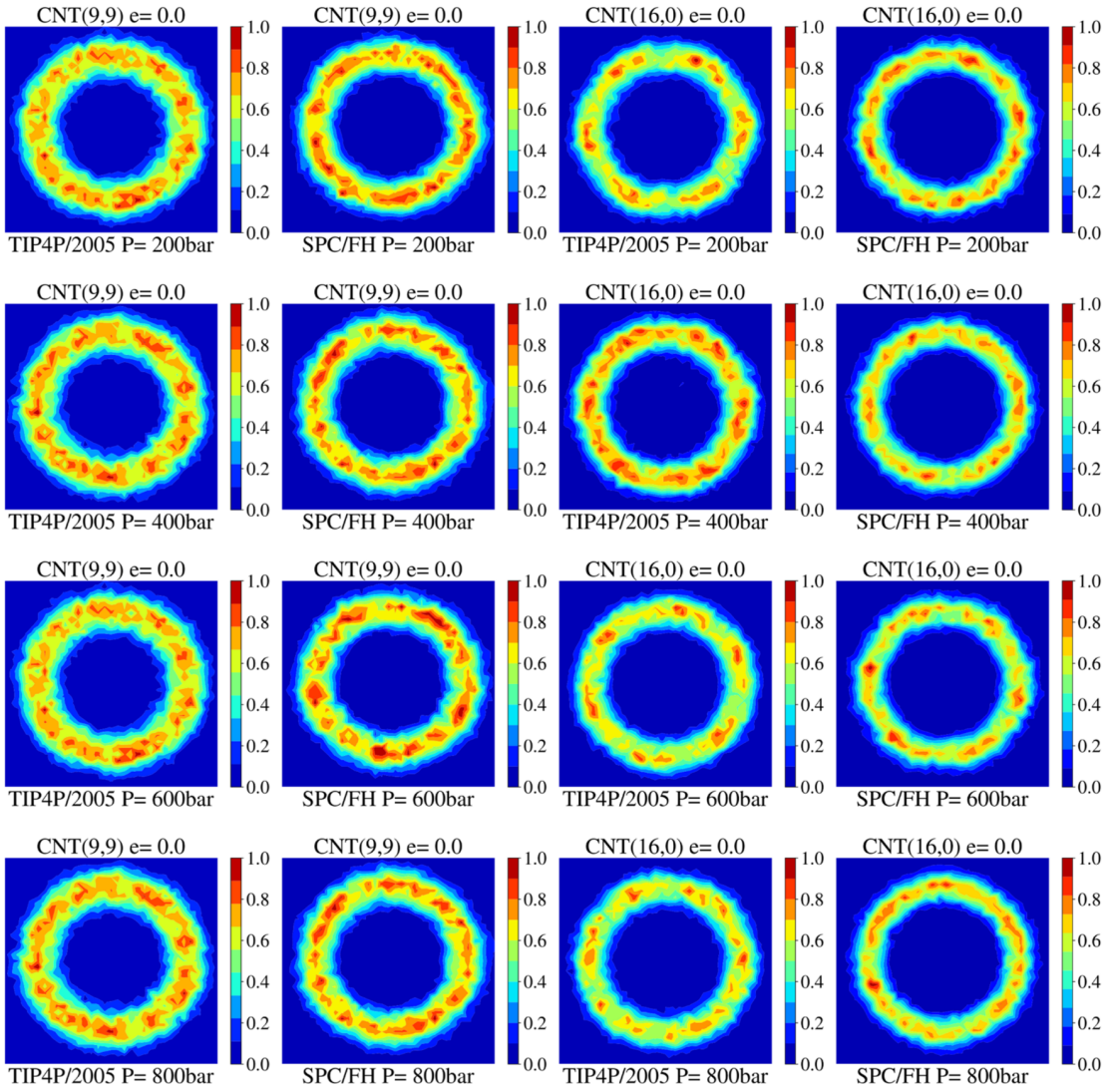

Figure 5. Density maps in the *xy*-direction for the carbon nanotubes (9,9) and (16,0) perfect P(n,m), and the comparison of the rigid TIP4P/2005 and flexible SPC/FH water models. Dark blue regions have a low probability of finding water molecules, while red regions have a high probability of finding water molecules.

competition between the pressure and the local arrangements that attempt to make the water molecules form a single file.

The behavior with pressure is linear for all three cases. The nanotube deformation does not change the linear regime but decreases the flow, particularly for larger pressures. This decrease can be attributed to the introduction of additional stress due to deformation. Figure 3b also shows the flow rate versus pressure, but for the SPC/FH model, the small deformation increases the flow rate, possibly because the hydrogen bonds adapt to enhance mobility. Larger deformations lead to an increase of stress and the mobility decreases.

Figure 3c illustrates the flow rate versus pressure for the (12,0) zigzag nanotube for the TIP4P/2005 model for the perfect and two cases of kneaded nanotubes. As observed in the perfect nanotube case,[103] the flow for the water in the armchair is larger than that in the zigzag nanotubes. The small deformation does not affect the flow rate. The same behavior is observed for the flexible SPC/FH shown in Figure 3d.

This result seems to reinforce the assumption that the large enhancement factor observed for water in armchair nanotubes is due to the spiral path the water molecules perform. Any deformation, that disrupts the spiral path, decreases the flow in the case of armchair nanotubes.

In the case of the (16,0) zigzag nanotube, the flow, illustrated in Figure 4a,b, shows the water flux versus pressure for an armchair (9,9) nanotube for the TIP4*P*/2005 and SPC/FH models for the perfect and two cases of kneaded nanotubes. In this diameter, both the diffusion[87] and enhancement factors[3] show a decrease when compared with smaller and larger nanotube diameters, which is attributed to the transition between a single line of water at smaller diameters to a single spiral of water molecules. In the case of flow, both TIP4P/2005 and SPC/FH are strongly affected by the deformation. SPC/FH due to the flexibility of the hydrogen bonds shows a larger mobility when compared with the rigid TIP4P/2005 model.

Figure 4c,d for the TIP4*P*/2005 and SPC/FH models shows an increase in water mobility when compared with the equivalent armchair nanotube. Even though in general water is more mobile in armchair nanotubes,[103] results for diffusion[14] show that the ring-like structure observed in the (16,0) is more mobile than the spiral-like organization seen in the (9,9) case.

https://doi.org/10.1021/acs.jpcb.3c02889
J. Phys. Chem. B 2023, 127, 8634−8643

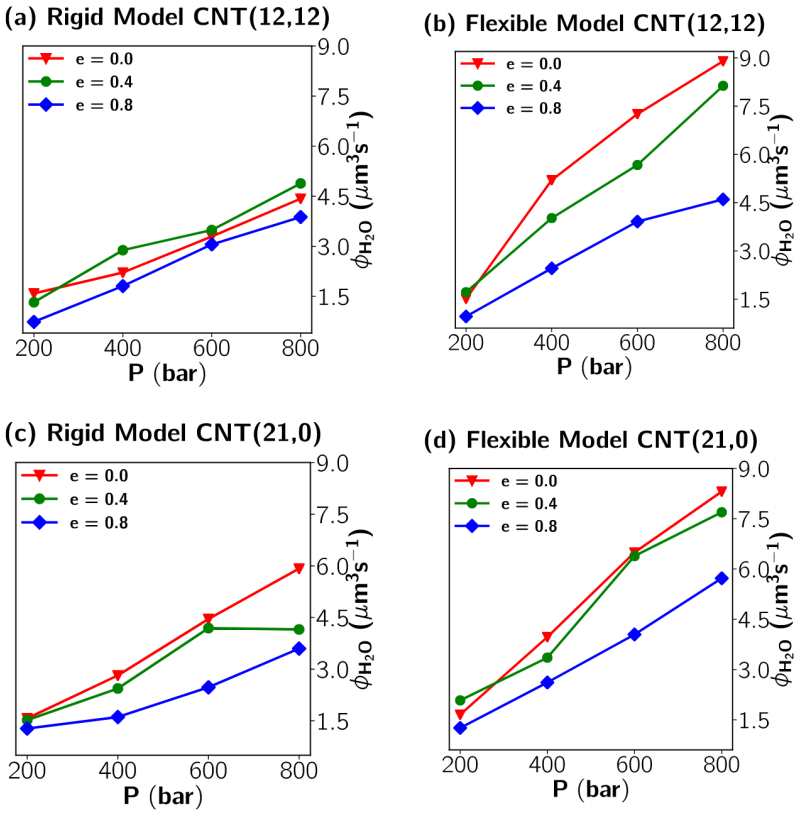

Figure 6. Flow rate as a function of the pressure gradient applied to the carbon nanotubes, (12,12) and (21,0), perfect P(n,m) with e = 0.0 and kneaded K(n,m) with e = 0.4 and 0.8 for rigid TIP4P/2005 and flexible SPC/FH water models.

The larger mobility observed for the flexible model is not surprising. It indicates a better accommodation of the hydrogen bonds.

For the perfect CNT (9,9) and (16,0) illustrated in Figure 5, water forms similar structures regardless of the wall. The two models of water adapt to the applied pressures, forming the same structural arrangement in both cases, causing the water to move with the same structure. An increase in the pressure applied to the systems would favor the formation process of hydrogen bonds; therefore, the effect of the nanotube structure would be predominant in the water flow. This phenomenon explains the low water flow found for these diameters.

For the CNT(12,12) and CNT(21,0) carbon nanotubes shown in Figure 6, as the pressure increases, rapid progress of water flow can be observed for both water models. The improvement in water flow as a function of the diameter of carbon nanotubes and the imposition of flexibility on water molecules is remarkable. By increasing the diameter of the cylindrical pore section, matching the membranes with the CNTs (12,12) and (21,0), the increase in water flux notably increases almost twice for the SPC/FH compared to the TIP4P/2005, indicating a strong dependence not only on the membrane diameter but also on the water model. For the SPC/FH model, this expressive increase in flow is due to the difference in connection and angle length and to the characteristic flexibility of the model. Another fact that explains this phenomenon is the increase in the space available for water molecules to pass each other. At larger CNT diameters, fluid−fluid interactions became more important as the CNT internal surface area to fluid volume ratio decreased.

CONCLUSIONS

We investigated the influence of deformations on carbon nanotubes with different chiralities and subjected to different pressure gradients for the transport of confined water, which helped to understand the relevance of the water model and these defects in improving the flow. We considered the TIP4P/2005 and SPC/FH models for the study.

The simulations showed how deformations on the carbon nanotube cross section affect the internal flow dynamics. The inclusion of deformations in tubes of smaller diameters (7,7) and (12,0) tends to considerably reduce the fluid velocity for larger deformations. The flow rate is further affected by a decrease in the overall density of the fluid caused by the presence of deformations. For large deformations, e = 0.8, the inclusion of strains disrupts the smooth, continuous potential energy landscape that a CNT provides, causing greater pressure losses along it, and reducing the overall fluid velocity.

The overall observation indicates that flow enhancement factors exhibit a considerable reduction when subjected to substantial degrees of deformation. However, there are specific cases in which tubes with diameters measuring 12.2 and 12.4 Å demonstrate an opposite trend, with flow rates tending to increase as the level of deformation rises. Water transport is not strongly affected by CNT chirality for different diameters and strains for both models, except for CNTs (9,9) and (16,0). This diameter is quite different compared to smaller and larger nanotubes because only a layer of water close to the wall is formed. This layer of water behaves quite differently depending on the chirality. The higher value deformations, in general, showed much less flow when compared to that of the perfect nanotube. The number of molecules passing through the pore

https://doi.org/10.1021/acs.jpcb.3c02889
J. Phys. Chem. B 2023, 127, 8634−8643

gradually decreases with an increase in the degree of deformation. In some cases, the flow did not show any significant variation. When the rate at which water molecules pass through the nanochannels is analyzed, the values found for the different diameters suggest that carbon nanotube membranes apparently can be competitive systems with currently existing water filtration processes.

These results indicate that carbon nanotube membranes are promising for use as filters for impure water or saline water, although more studies are needed to categorically affirm their viability. Furthermore, advances in experimental measurements of nanoconfined water will lead to more accurate models of water in carbon nanotube simulations. Currently, atomistic water models can provide a reasonable range of results for the flow of water through CNTs. Understanding the impacts of simulation choices aids in the analysis of past results and improves the design of future simulation studies.

AUTHOR INFORMATION

Corresponding Author

Bruno H. S. Mendonça − *Departamento de Física, ICEX, Universidade Federal de Minas Gerais, Belo Horizonte 30123-970 MG, Brazil;* orcid.org/0000-0001-7782-0515; Email: brunnohennrique13@gmail.com

Authors

Elizane E. de Moraes − *Instituto de Física, Universidade Federal da Bahia, Salvador 40210-340 BA, Brazil;* orcid.org/0000-0001-5208-2835

Alexsandro Kirch − *Instituto de Física, Universidade de São Paulo, São Paulo 05315-970 SP, Brazil*

Ronaldo J. C. Batista − *Departamento de Física, Universidade Federal de Ouro Preto, Ouro Preto 35400-000 MG, Brazil*

Alan B. de Oliveira − *Departamento de Física, Universidade Federal de Ouro Preto, Ouro Preto 35400-000 MG, Brazil*

Marcia C. Barbosa − *Instituto de Física, Universidade Federal do Rio Grande do Sul, Porto Alegre 91501-970 RS, Brazil;* orcid.org/0000-0001-5663-6102

Hélio Chacham − *Departamento de Física, ICEX, Universidade Federal de Minas Gerais, Belo Horizonte 30123-970 MG, Brazil;* orcid.org/0000-0001-5041-9094

Complete contact information is available at: https://pubs.acs.org/10.1021/acs.jpcb.3c02889

Notes

The authors declare no competing financial interest.

ACKNOWLEDGMENTS

This work is funded by the Brazilian scientific agency Conselho Nacional de Desenvolvimento Científico e Tecnológico (CNPq) and the Brazilian Institute of Science and Technology (INCT) in Carbon Nanomaterials with collaboration and computational support from Universidade Federal de Minas Gerais (UFMG), Universidade Federal de Ouro Preto (UFOP), Universidade Federal da Bahia (UFBA), and Universidade de So Paulo (USP). A.B.d.O. and R.J.C.B. thank the science agencies FAPEMIG and PROPPI-UFOP for financial support. B.H.S.M. wishes to acknowledge Joo P. K. Abal (UFRGS) for discussions and theoretical contributions. The authors acknowledge the National Laboratory for Scientific Computing (LNCC/MCTI, Brazil) for providing HPC resources of the SDumont supercomputer, which have contributed to the research results reported within this paper. URL: http://sdumont.lncc.br.

REFERENCES

(1) Hummer, G.; Rasaiah, J.; Noworyta, J. Nanoscale hydrodynamics: enhanced flow in carbon nanotubes. *Nature* **2001**, *414*, No. 188.

(2) Holt, J. K.; Park, H. G.; Wang, Y.; Stadermann, M.; Artyukhin, A. B.; Grigoropoulos, C. P.; Noy, A.; Bakajin, O. Fast mass transport through sub-2-nanometer carbon nanotubes. *Science* **2006**, *312*, 1034−1037.

(3) Qin, X.; Yuan, Q.; Zhao, Y.; Xie, S.; Liu, Z. Measurement of the rate of water translocation through carbon nanotubes. *Nano Lett.* **2011**, *11*, 2173−2177.

(4) Hummer, G.; Rasaiah, J. C.; Noworyta, J. P. Water conduction through the hydrophobic channel of a carbon nanotube. *Nature* **2001**, *414*, 188−190.

(5) Bordin, J. R.; Diehl, A.; Barbosa, M. C. Relation between flow enhancement factor and structure for core-softened fluids inside nanotubes. *J. Phys. Chem. B* **2013**, *117*, 7047−7056.

(6) Whitby, M.; Quirke, N. Fluid flow in carbon nanotubes and nanopipes. *Nat. Nanotechnol.* **2007**, *2*, 87−94.

(7) Wu, J.; Paudel, K. S.; Strasinger, C.; Hammell, D.; Stinchcomb, A. L.; Hinds, B. J. Programmable transdermal drug delivery of nicotine using carbon nanotube membranes. *Proc. Natl. Acad. Sci. U.S.A.* **2010**, *107*, 11698−11702.

(8) Joseph, S.; Mashl, R. J.; Jakobsson, E.; Aluru, N. Electrolytic transport in modified carbon nanotubes. *Nano Lett.* **2003**, *3*, 1399−1403.

(9) Kiani, F.; Khosravi, T.; Moradi, F.; Rahbari, P.; Aghaei, M.; Arabi, M.; Tajik, H.; Kalantarinejad, R. Computational Investigation of Carbon NanotubesEnhanced Membrane for Water Desalination Based on Flux and Rejection Characteristics. *J. Comput. Theor. Nanosci.* **2014**, *11*, 1237−1243.

(10) Corry, B. Designing carbon nanotube membranes for efficient water desalination. *J. Phys. Chem. B* **2008**, *112*, 1427−1434.

(11) Sholl, D. S.; Johnson, J. K. Making high-flux membranes with carbon nanotubes. *Science* **2006**, *312*, 1003−1004.

(12) Yang, D.-C.; Castellano, R. J.; Silvy, R. P.; Lageshetty, S. K.; Praino, R. F.; Fornasiero, F.; Shan, J. W. Fast Water Transport through Subnanometer Diameter Vertically Aligned Carbon Nanotube Membranes. *Nano Lett.* **2023**, *23*, 4956−4964, DOI: 10.1021/acs.nanolett.3c00797.

(13) Secchi, E.; Marbach, S.; Niguès, A.; Stein, D.; Siria, A.; Bocquet, L. Massive radius-dependent flow slippage in carbon nanotubes. *Nature* **2016**, *537*, 210−213.

(14) Plimpton, S. Fast parallel algorithms for short-range molecular dynamics. *J. Comput. Phys.* **1995**, *117*, 1−19.

(15) Berendsen, H. J. C.; Postma, J. P.; van Gunsteren, W. F.; Hermans, J.Interaction Models for Water in Relation to Protein Hydration. In *The Jerusalem Symposia on Quantum Chemistry and Biochemistry*; Springer, 1981; Vol. *14*, pp 331−342.

(16) Teleman, O.; Jönsson, B.; Engström, S. A molecular dynamics simulation of a water model with intramolecular degrees of freedom. *Mol. Phys.* **1987**, *60*, 193−203.

(17) Abascal, J. L. F.; Vega, C. A general purpose model for the condensed phases of water: TIP4P/2005. *J. Chem. Phys.* **2005**, *123*, No. 234505.

(18) Kaminski, G. A.; Friesner, R. A.; Tirado-Rives, J.; Jorgensen, W. L. Evaluation and reparametrization of the OPLS-AA force field for proteins via comparison with accurate quantum chemical calculations on peptides. *J. Phys. Chem. B* **2001**, *105*, 6474−6487.

(19) Horn, H. W.; Swope, W. C.; Pitera, J. W.; Madura, J. D.; Dick, T. J.; Hura, G. L.; Head-Gordon, T. Development of an improved four-site water model for biomolecular simulations: TIP4P-Ew. *J. Chem. Phys.* **2004**, *120*, 9665−9678.

(20) Jorgensen, W. L.; Chandrasekhar, J.; Madura, J. D.; Impey, R. W.; Klein, M. L. Comparison of simple potential functions for simulating liquid water. *J. Chem. Phys.* **1983**, *79*, 926−935.

(21) Mahoney, M. W.; Jorgensen, W. L. A five-site model for liquid water and the reproduction of the density anomaly by rigid, nonpolarizable potential functions. *J. Chem. Phys.* **2000**, *112*, 8910−8922.
(22) Vega, C.; Abascal, J. Relation between the melting temperature and the temperature of maximum density for the most common models of water. *J. Chem. Phys.* **2005**, *123*, No. 144504.
(23) López-Lemus, J.; Chapela, G. A.; Alejandre, J. Effect of flexibility on surface tension and coexisting densities of water. *J. Chem. Phys.* **2008**, *128*, No. 174703.
(24) Alejandre, J.; Chapela, G. A.; Bresme, F.; Hansen, J.-P. The short range anion-H interaction is the driving force for crystal formation of ions in water. *J. Chem. Phys.* **2009**, *130*, No. 174505.
(25) Zhang, L.; Wang, H.; Car, R.; Weinan, E. Phase diagram of a deep potential water model. *Phys. Rev. Lett.* **2021**, *126*, No. 236001.
(26) Wallqvist, A.; Teleman, O. Properties of flexible water models. *Mol. Phys.* **1991**, *74*, 515−533.
(27) Tocci, G.; Bilichenko, M.; Joly, L.; Iannuzzi, M. Ab initio nanofluidics: disentangling the role of the energy landscape and of density correlations on liquid/solid friction. *Nanoscale* **2020**, *12*, 10994−11000.
(28) Andrade, M. F. C.; Pham, T. A. Probing Confinement Effects on the Infrared Spectra of Water with deep Potential Molecular Dynamics Simulations. *J. Phys. Chem. Lett.* **2023**, *14*, 5560−5566.
(29) Babin, V.; Leforestier, C.; Paesani, F. Development of a "first principles" water potential with flexible monomers: Dimer potential energy surface, VRT spectrum, and second virial coefficient. *J. Chem. Theory Comput.* **2013**, *9*, 5395−5403.
(30) Babin, V.; Medders, G. R.; Paesani, F. Development of a "first principles" water potential with flexible monomers. II: Trimer potential energy surface, third virial coefficient, and small clusters. *J. Chem. Theory Comput.* **2014**, *10*, 1599−1607.
(31) Medders, G. R.; Babin, V.; Paesani, F. Development of a "first-principles" water potential with flexible monomers. III. Liquid phase properties. *J. Chem. Theory Comput.* **2014**, *10*, 2906−2910.
(32) Das, A. K.; Urban, L.; Leven, I.; Loipersberger, M.; Aldossary, A.; Head-Gordon, M.; Head-Gordon, T. Development of an advanced force field for water using variational energy decomposition analysis. *J. Chem. Theory Comput.* **2019**, *15*, 5001−5013.
(33) Liu, C.; Piquemal, J.-P.; Ren, P. AMOEBA+ classical potential for modeling molecular interactions. *J. Chem. Theory Comput.* **2019**, *15*, 4122−4139.
(34) Liu, C.; Piquemal, J.-P.; Ren, P. Implementation of geometry-dependent charge flux into the polarizable AMOEBA+ potential. *J. Phys. Chem. Lett.* **2020**, *11*, 419−426.
(35) Rackers, J. A.; Silva, R. R.; Wang, Z.; Ponder, J. W. Polarizable water potential derived from a model electron density. *J. Chem. Theory Comput.* **2021**, *17*, 7056−7084.
(36) Rieth, A. J.; Hunter, K. M.; Dincă, M.; Paesani, F. Hydrogen bonding structure of confined water templated by a metal-organic framework with open metal sites. *Nat. Commun.* **2019**, *10*, No. 4771.
(37) Wagner, J. C.; Hunter, K. M.; Paesani, F.; Xiong, W. Water capture mechanisms at zeolitic imidazolate framework interfaces. *J. Am. Chem. Soc.* **2021**, *143*, 21189−21194.
(38) Lambros, E.; Paesani, F. How good are polarizable and flexible models for water: Insights from a many-body perspective. *J. Chem. Phys.* **2020**, *153*, No. 060901.
(39) Paesani, F. Getting the right answers for the right reasons: Toward predictive molecular simulations of water with many-body potential energy functions. *Acc. Chem. Res.* **2016**, *49*, 1844−1851.
(40) Richardson, J. O.; Pérez, C.; Lobsiger, S.; Reid, A. A.; Temelso, B.; Shields, G. C.; Kisiel, Z.; Wales, D. J.; Pate, B. H.; Althorpe, S. C. Concerted hydrogen-bond breaking by quantum tunneling in the water hexamer prism. *Science* **2016**, *351*, 1310−1313.
(41) Cole, W. T.; Farrell, J. D.; Wales, D. J.; Saykally, R. J. Structure and torsional dynamics of the water octamer from THz laser spectroscopy near 215 μm. *Science* **2016**, *352*, 1194−1197.
(42) Mallory, J. D.; Mandelshtam, V. A. Diffusion Monte Carlo studies of MB-pol (H2O) 2- 6 and (D2O) 2- 6 clusters: Structures and binding energies. *J. Chem. Phys.* **2016**, *145*, No. 064308, DOI: 10.1063/1.4960610.
(43) Videla, P. E.; Rossky, P. J.; Laria, D. Communication: Isotopic effects on tunneling motions in the water trimer. *J. Chem. Phys.* **2016**, *144*, No. 061101, DOI: 10.1063/1.4941701.
(44) Brown, S. E.; Gotz, A. W.; Cheng, X.; Steele, R. P.; Mandelshtam, V. A.; Paesani, F. Monitoring water clusters "melt" through vibrational spectroscopy. *J. Am. Chem. Soc.* **2017**, *139*, 7082−7088.
(45) Vaillant, C. L.; Cvitaš, M. T. Rotation-tunneling spectrum of the water dimer from instanton theory. *Phys. Chem. Chem. Phys.* **2018**, *20*, 26809−26813.
(46) Vaillant, C. L.; Wales, D.; Althorpe, S. Tunneling splittings from path-integral molecular dynamics using a Langevin thermostat. *J. Chem. Phys.* **2018**, *148*, No. 34102, DOI: 10.1063/1.5029258.
(47) Schmidt, M.; Roy, P.-N. Path integral molecular dynamic simulation of flexible molecular systems in their ground state: Application to the water dimer. *J. Chem. Phys.* **2018**, *148*, No. 124116, DOI: 10.1063/1.5017532.
(48) Bishop, K. P.; Roy, P.-N. Quantum mechanical free energy profiles with post-quantization restraints: Binding free energy of the water dimer over a broad range of temperatures. *J. Chem. Phys.* **2018**, *148*, No. 102303, DOI: 10.1063/1.4986915.
(49) Videla, P. E.; Rossky, P. J.; Laria, D. Isotopic equilibria in aqueous clusters at low temperatures: Insights from the MB-pol many-body potential. *J. Chem. Phys.* **2018**, *148*, No. 084303, DOI: 10.1063/1.5019377.
(50) Samala, N. R.; Agmon, N. Temperature dependence of intramolecular vibrational bands in small water clusters. *J. Phys. Chem. B* **2019**, *123*, 9428−9442.
(51) Cvitaš, M. T.; Richardson, J. O. Quantum tunnelling pathways of the water pentamer. *Phys. Chem. Chem. Phys.* **2020**, *22*, 1035−1044.
(52) Reddy, S. K.; Straight, S. C.; Bajaj, P.; Pham, C. H.; Riera, M.; Moberg, D. R.; Morales, M. A.; Knight, C.; Götz, A. W.; Paesani, F. On the accuracy of the MB-pol many-body potential for water: Interaction energies, vibrational frequencies, and classical thermodynamic and dynamical properties from clusters to liquid water and ice. *J. Chem. Phys.* **2016**, *145*, No. 194504, DOI: 10.1063/1.4967719.
(53) Gartner, T. E., III; Hunter, K. M.; Lambros, E.; Caruso, A.; Riera, M.; Medders, G. R.; Panagiotopoulos, A. Z.; Debenedetti, P. G.; Paesani, F. Anomalies and local structure of liquid water from boiling to the supercooled regime as predicted by the many-body MB-pol model. The. *J. Phys. Chem. Lett.* **2022**, *13*, 3652−3658.
(54) Medders, G. R.; Paesani, F. Infrared and Raman spectroscopy of liquid water through "first-principles" many-body molecular dynamics. *J. Chem. Theory Comput.* **2015**, *11*, 1145−1154.
(55) Straight, S. C.; Paesani, F. Exploring electrostatic effects on the hydrogen bond network of liquid water through many-body molecular dynamics. *J. Phys. Chem. B* **2016**, *120*, 8539−8546.
(56) Reddy, S. K.; Moberg, D. R.; Straight, S. C.; Paesani, F. Temperature-dependent vibrational spectra and structure of liquid water from classical and quantum simulations with the MB-pol potential energy function. *J. Chem. Phys.* **2017**, *147*, No. 244504, DOI: 10.1063/1.5006480.
(57) Hunter, K. M.; Shakib, F. A.; Paesani, F. Disentangling coupling effects in the infrared spectra of liquid water. *J. Phys. Chem. B* **2018**, *122*, 10754−10761.
(58) Sun, Z.; Zheng, L.; Chen, M.; Klein, M. L.; Paesani, F.; Wu, X. Electron-hole theory of the effect of quantum nuclei on the X-ray absorption spectra of liquid water. *Phys. Rev. Lett.* **2018**, *121*, No. 137401.
(59) Gaiduk, A. P.; Pham, T. A.; Govoni, M.; Paesani, F.; Galli, G. Electron affinity of liquid water. *Nat. Commun.* **2018**, *9*, No. 247.
(60) Cruzeiro, V. W. D.; Wildman, A.; Li, X.; Paesani, F. Relationship between hydrogen-bonding motifs and the 1b1 splitting in the x-ray emission spectrum of liquid water. *J. Phys. Chem. Lett.* **2021**, *12*, 3996−4002.
(61) Medders, G. R.; Paesani, F. Dissecting the molecular structure of the air/water interface from quantum simulations of the sum-

frequency generation spectrum. *J. Am. Chem. Soc.* **2016**, *138*, 3912−3919.
(62) Moberg, D. R.; Straight, S. C.; Paesani, F. Temperature dependence of the air/water interface revealed by polarization sensitive sum-frequency generation spectroscopy. *J. Phys. Chem. B* **2018**, *122*, 4356−4365.
(63) Sun, S.; Tang, F.; Imoto, S.; Moberg, D. R.; Ohto, T.; Paesani, F.; Bonn, M.; Backus, E. H.; Nagata, Y. Orientational distribution of free OH groups of interfacial water is exponential. *Phys. Rev. Lett.* **2018**, *121*, No. 246101.
(64) Sengupta, S.; Moberg, D. R.; Paesani, F.; Tyrode, E. Neat water-vapor interface: Proton continuum and the nonresonant background. *J. Phys. Chem. Lett.* **2018**, *9*, 6744−6749.
(65) Muniz, M. C.; Gartner, T. E.; Riera, M.; Knight, C.; Yue, S.; Paesani, F.; Panagiotopoulos, A. Z. Vapor−liquid equilibrium of water with the MB-pol many-body potential. *J. Chem. Phys.* **2021**, *154*, No. 211103, DOI: 10.1063/5.0050068.
(66) Pham, C. H.; Reddy, S. K.; Chen, K.; Knight, C.; Paesani, F. Many-body interactions in ice. *J. Chem. Theory Comput.* **2017**, *13*, 1778−1784.
(67) Moberg, D. R.; Straight, S. C.; Knight, C.; Paesani, F. Molecular origin of the vibrational structure of ice Ih. *J. Phys. Chem. Lett.* **2017**, *8*, 2579−2583.
(68) Moberg, D. R.; Sharp, P. J.; Paesani, F. Molecular-level interpretation of vibrational spectra of ordered ice phases. *J. Phys. Chem. B* **2018**, *122*, 10572−10581.
(69) Moberg, D. R.; Becker, D.; Dierking, C. W.; Zurheide, F.; Bandow, B.; Buck, U.; Hudait, A.; Molinero, V.; Paesani, F.; Zeuch, T. The end of ice I. *Proc. Natl. Acad. Sci. U.S.A.* **2019**, *116*, 24413−24419.
(70) Bore, S. L.; Paesani, F. Realistic phase diagram of water from "first principles" data-driven quantum simulations. *Nat. Commun.* **2023**, *14*, No. 3349.
(71) Hunter, K. M.; Wagner, J. C.; Kalaj, M.; Cohen, S. M.; Xiong, W.; Paesani, F. Simulation meets experiment: unraveling the properties of water in metal-organic frameworks through vibrational spectroscopy. *J. Phys. Chem. C* **2021**, *125*, 12451−12460.
(72) Ho, C.-H.; Valentine, M. L.; Chen, Z.; Xie, H.; Farha, O.; Xiong, W.; Paesani, F. Structure and thermodynamics of water adsorption in NU-1500-Cr. *Commun. Chem.* **2023**, *6*, No. 70.
(73) Fuentes-Azcatl, R.; Barbosa, M. C. Thermodynamic and dynamic anomalous behavior in the TIP4P/ε water model. *Phys. A* **2016**, *444*, 86−94.
(74) González, M. A.; Abascal, J. L. A flexible model for water based on TIP4P/2005. *J. Chem. Phys.* **2011**, *135*, No. 224516, DOI: 10.1063/1.3663219.
(75) Holz, M.; Heil, S. R.; Sacco, A. Temperature-dependent self-diffusion coefficients of water and six selected molecular liquids for calibration in accurate 1H NMR PFG measurements. *Phys. Chem. Chem. Phys.* **2000**, *2*, 4740−4742.
(76) Kirch, A.; de Almeida, J. M.; Miranda, C. R. Multilevel molecular modeling approach for a rational design of ionic current sensors for nanofluidics. *J. Chem. Theory Comput.* **2018**, *14*, 3113−3120.
(77) de Oliveira, A. B.; Chacham, H.; Soares, J. S.; Manhabosco, T. M.; de Resende, H. F.; Batista, R. J. Vibrational G peak splitting in laterally functionalized single wall carbon nanotubes: Theory and molecular dynamics simulations. *Carbon* **2016**, *96*, 616−621.
(78) Umeno, Y.; Kitamura, T.; Kushima, A. Theoretical analysis on electronic properties of zigzag-type single-walled carbon nanotubes under radial deformation. *Comput. Mater. Sci.* **2004**, *30*, 283−287.
(79) Sisto, T. J.; Zakharov, L. N.; White, B. M.; Jasti, R. Towards pi-extended cycloparaphenylenes as seeds for CNT growth: investigating strain relieving ring-openings and rearrangements. *Chem. Sci.* **2016**, *7*, 3681−3688.
(80) Kroes, J. M. H.; Pietrucci, F.; Van Duin, A. C.; Andreoni, W. Atom vacancies on a carbon nanotube: to what extent can we simulate their effects? *J. Chem. Theory Comput.* **2015**, *11*, 3393−3400.
(81) Xu, B.; Li, Y.; Park, T.; Chen, X. Effect of wall roughness on fluid transport resistance in nanopores. *J. Chem. Phys.* **2011**, *135*, No. 144703.
(82) Secchi, E.; Marbach, S.; Niguès, A.; Stein, D.; Siria, A.; Bocquet, L. Massive radius-dependent flow slippage in carbon nanotubes. *Nature* **2016**, *537*, 210−213.
(83) Belin, C.; Joly, L.; Detcheverry, F. Optimal shape of entrances for a frictionless nanochannel. *Phys. Rev. Fluids* **2016**, *1*, No. 054103.
(84) Mendonça, B. H.; de Moraes, E. E.; Batista, R. J.; de Oliveira, A. B.; Barbosa, M. C.; Chacham, H. Water diffusion in carbon nanotubes for rigid and flexible models. *J. Phys. Chem. C* **2023**, *127*, 9769−9778, DOI: 10.1021/acs.jpcc.3c00490.
(85) Huang, C.; Nandakumar, K.; Choi, P. Y.; Kostiuk, L. W. Molecular dynamics simulation of a pressure-driven liquid transport process in a cylindrical nanopore using two self-adjusting plates. *J. Chem. Phys.* **2006**, *124*, No. 234701.
(86) Mendonça, B. H. S.; de Freitas, D. N.; Köhler, M. H.; Batista, R. J.; Barbosa, M. C.; de Oliveira, A. B. Diffusion behaviour of water confined in deformed carbon nanotubes. *Phys. A* **2019**, *517*, 491−498.
(87) Mendonça, B. H. S.; Ternes, P.; Salcedo, E.; de Oliveira, A. B.; Barbosa, M. C. Water diffusion in rough carbon nanotubes. *J. Chem. Phys.* **2020**, *152*, No. 024708.
(88) Mendonça, B. H. S.; Ternes, P.; Salcedo, E.; de Oliveira, A. B.; Barbosa, M. C. Water diffusion in carbon nanotubes: Interplay between confinement, surface deformation, and temperature. *J. Chem. Phys.* **2020**, *153*, No. 244504.
(89) Ryckaert, J.-P.; Ciccotti, G.; Berendsen, H. J. Numerical integration of the cartesian equations of motion of a system with constraints: molecular dynamics of n-alkanes. *J. Comput. Phys.* **1977**, *23*, 327−341.
(90) Lennard-Jones, J. E. Cohesion. *Proc. Phys. Soc.* **1931**, *43*, 461−482.
(91) Ostler, D.; Kannam, S. K.; Daivis, P. J.; Frascoli, F.; Todd, B. Electropumping of water in functionalized carbon nanotubes using rotating electric fields. *J. Phys. Chem. C* **2017**, *121*, 28158−28165.
(92) Nosé, S. A molecular dynamics method for simulations in the canonical ensemble. *Mol. Phys.* **1984**, *52*, 255−268.
(93) Agrawal, K. V.; Drahushuk, L. W.; Strano, M. S. Observation and analysis of the Coulter effect through carbon nanotube and graphene nanopores. *Philos. Trans. R. Soc., A* **2016**, *374*, No. 20150357.
(94) Rikhtehgaran, S.; Lohrasebi, A. Water desalination by a designed nanofilter of graphene-charged carbon nanotube: A molecular dynamics study. *Desalination* **2015**, *365*, 176−181.
(95) Ang, E. Y. M.; Ng, T. Y.; Yeo, J.; Lin, R.; Liu, Z.; Geethalakshmi, K. Effects of CNT size on the desalination performance of an outer-wall CNT slit membrane. *Phys. Chem. Chem. Phys.* **2018**, *20*, 13896−13902.
(96) de Freitas, D. N.; Mendonça, B. H. S.; Köhler, M. H.; Barbosa, M. C.; Matos, M. J.; Batista, R. J.; de Oliveira, A. B. Water diffusion in carbon nanotubes under directional electric frields: Coupling between mobility and hydrogen bonding. *Chem. Phys.* **2020**, *537*, No. 110849.
(97) Zhao, K.; Wu, H.; Han, B. Negative effect of nanoconfinement on water transport across nanotube membranes. *J. Chem. Phys.* **2017**, *147*, No. 164705.
(98) Sahu, P.; Ali, S. M.; Shenoy, K. *Self Diffusion and Wetting Transition of Fluids in Carbon Nanotubes*, AIP Conference Proceedings; AIP Publishing, 2016; p 110050.
(99) Wang, R.; Chen, D.; Wang, Q.; Ying, Y.; Gao, W.; Xie, L. Recent advances in applications of carbon nanotubes for desalination: A review. *Nanomaterials* **2020**, *10*, No. 1203.
(100) Bernardina, S. D.; Paineau, E.; Brubach, J.-B.; Judeinstein, P.; Rouzière, S.; Launois, P.; Roy, P. Water in carbon nanotubes: the peculiar hydrogen bond network revealed by infrared spectroscopy. *J. Am. Chem. Soc.* **2016**, *138*, 10437−10443.
(101) Tao, J.; Song, X.; Zhao, T.; Zhao, S.; Liu, H. Confinement effect on water transport in CNT membranes. *Chem. Eng. Sci.* **2018**, *192*, 1252−1259.

(102) Losey, J.; Kannam, S. K.; Todd, B.; Sadus, R. J. Flow of water through carbon nanotubes predicted by different atomistic water models. *J. Chem. Phys.* **2019**, *150*, No. 194501.
(103) Sam, A.; Prasad, K. V.; Sathian, S. P. Water flow in carbon nanotubes: the role of tube chirality. *Phys. Chem. Chem. Phys.* **2019**, *21*, 6566−6573.
(104) Thomas, J. A.; McGaughey, A. J. H.; Kuter-Arnebeck, O. Pressure-driven water flow through carbon nanotubes: Insights from molecular dynamics simulation. *Int. J. Therm. Sci.* **2010**, *49*, 281−289.
(105) Lv, F.; Fang, C.; Su, J. Enhanced water transport through a carbon nanotube controlled by the lateral pressure. *Nanotechnology* **2019**, *30*, No. 245707.
(106) Zhao, Y.; Su, J. Coupling Transport of Water and Ions through a Carbon Nanotube in a Pressure Difference: The Relation between Dynamics and Ion Structures. *J. Phys. Chem. C* **2018**, *122*, No. 22178.

https://doi.org/10.1021/acs.jpcb.3c02889
J. Phys. Chem. B 2023, 127, 8634−8643